Polymer 50 (2009) 1566–1576

Contents lists available at ScienceDirect

Polymer

journal homepage: www.elsevier.com/locate/polymer

Ultra small-angle X-ray scattering studies on structural changes in micrometers upon uniaxial stretching of segmented polyurethaneureas

Shinichi Sakurai [a,*], Hidekazu Yoshida [a], Fumio Hashimoto [b], Miaki Shibaya [b], Hideaki Ishihara [b,1], Nori Yoshihara [c], Shotaro Nishitsuji [d], Mikihito Takenaka [d]

[a] Department of Polymer Science and Engineering, Graduate School of Science and Technology, Kyoto Institute of Technology, Matsugasaki, Sakyo-ku, Kyoto 606-8585, Japan
[b] Division of Advanced Fibro-Science, Graduate School of Science and Technology, Kyoto Institute of Technology, Matsugasaki, Sakyo-ku, Kyoto 606-8585, Japan
[c] Research Center, Toyobo Co., Ltd., 2-1-1 Katata, Otsu, Shiga 520-0292, Japan
[d] Department of Polymer Chemistry, Graduate School of Engineering, Kyoto University, Katsura, Kyoto 615-8510, Japan

ARTICLE INFO

Article history:
Received 23 September 2008
Received in revised form
21 December 2008
Accepted 26 December 2008
Available online 21 January 2009

Keywords:
Ultra small-angle X-ray scattering
Uniaxial stretching
Segmented polyurethaneureas

ABSTRACT

Ultra small-angle X-ray scattering (USAXS) experiments were conducted in order to examine structural changes in micrometers upon uniaxial stretching of elastomeric segmented polyurethaneureas at room temperature. It was possible to stretch the sample film up to $\alpha = 7.5$ without break, where α designates the stretching ratio. Around $\alpha = 6.5$ the sample became turbid, while it recovered transparency when the stress was removed. To understand this curious phenomenon, we conducted the USAXS experiments for the structural analyses in micrometers. Although a set of streaks appeared in the direction parallel to the stretching direction (SD) when the sample became turbid (around $\alpha = 7.2$), more interesting result is that a set of streaks appeared in the direction perpendicular to SD much earlier around $\alpha = 5.0$. Close examination of the scattering intensity profile revealed evolution of multiple interference peaks, which could be ascribed to the form factor of a lamellar particle. Since the streaks disappeared upon the removal of the stress, "lamellar particles" are considered to be crazes, which develop further into cracks in a subsequent stage. From the results of USAXS measurements, it is suggested that the lamellar-shaped crazes appeared around $\alpha = 5.0$ being oriented parallel to SD, and further stretching created other lamellar-shaped crazes being oriented perpendicular to SD, which are co-existing with the preceding parallel crazes.

1. Introduction

Segmented polyurethaneureas comprising hard and soft segments [1–7] have been widely used as materials featuring the prominent elastomeric property, for instance as elastic fibers [8]. More recently they have also been attracting interests for biomedical applications [9–11] and for development of nano-fibers [12]. It has been well known that the characteristic mechanical properties are originated from the nano-structures due to phase separation into hard and soft segment domains, and hence it is important to understand the structure–property relationship. To conduct structural analysis in nanometers, the small-angle X-ray scattering (SAXS) technique is generally used. Not only the static SAXS measurements [6,7,9–18], but also have been conducted in-situ measurements along with deformation [19–21]. Note here that measurements of two-dimensional SAXS (2D-SAXS) pattern are required to analyze structural changes and orientation of nano-structures along with the mechanical deformation, which are relevant to mechanical fatigue [14,17,22–25] and fracture [5,6]. Simultaneous measurements of 2D-SAXS with stress–strain behavior become popular nowadays and applied to studies for understanding of the structure–property relationship in polyurethanes [20,21].

As far as fatigue and fracture are concerned, the conventional SAXS apparatus is not satisfactory because it allows us to analyze structures only in several tens of nanometers. Analyses in much larger scales are sometime required, for instance for highly deformed elastomers where we are interested in craze formation, kinetics of crack propagation, and the overall process towards the macroscopic fracture. For this purpose, ultra small X-ray scattering (USAXS) apparatus [26,27], which has been recently settled in SPring-8 (Japan, Hyogo), is tremendously promising. This utilizes a quite long evacuated flight path to provide the sample-to-detector distance of about 150 m, covering the range of targeted

* Corresponding author. Tel.: +81 75 724 7864; fax: +81 75 724 7800.
E-mail addresses: shin@kit.jp (S. Sakurai), h-ishihara@ad.ryukoku.ac.jp (H. Ishihara).
[1] Present address: Ryukoku Extension Center, Ryukoku University, 1-5 Seta, Otsu, Shiga 520-2194, Japan.

0032-3861/$ – see front matter © 2009 Elsevier Ltd. All rights reserved.
doi:10.1016/j.polymer.2008.12.050

structures from 300 nm up to 2.0 μm. This range, which is referred sometime to as *forsaken dimension*, cannot be covered by small-angle light scattering (SALS) either. Since the range can be covered by the USAXS technique, one can obtain full range of scattering function (structure factor) without intermittence, giving significant contribution to nano-science and nano-technology.

In the current study, we applied the two-dimensional USAXS (2D-USAXS) technique to the structural analyses of the polyurethaneureas undergoing fracture under uniaxial stretching. The sample film could be stretched up to more than $\alpha = 7.5$ due to their excellent elastomeric property and from the intermediate stage the hard-segment domains were divided into fragments, where α designates stretching ratio. As a matter of fact, we observed whitening at approximately $\alpha = 6$–7. Therefore, we focused on the early stage of the uniaxial stretching where craze initiation and developments can be considered to have already set in because our preliminary experiments imply that the hard-segment domains undergo fragmentation at about $\alpha = 3.5$ where the sample film is still transparent. As shown schematically in Fig. 1, the so-called lamellar type hard-segment domains [16,19] suffer from microscopic fracture so that crazing sets in. To detect the onset, we should conduct in-situ measurements of the 2D-USAXS along with the sample stretching. Unfortunately, the in-situ measurements are not available because of insufficient intensity of the incident beam when measured at the end of the evacuated flight path, which is 240 m away from the insertion device (undulator) in the synchrotron storage ring. Simultaneous stress–strain measurements are not available, either. Therefore, we simply performed the 2D-USAXS measurements one by one with holding the sample at fixed stretching ratio, followed by subsequent stretching to the next destination of stretching ratio.

2. Experimental

2.1. Sample preparation

The polyurethaneurea samples were synthesized by the chain extension of MDI-terminated PTMG prepolymers, where MDI and

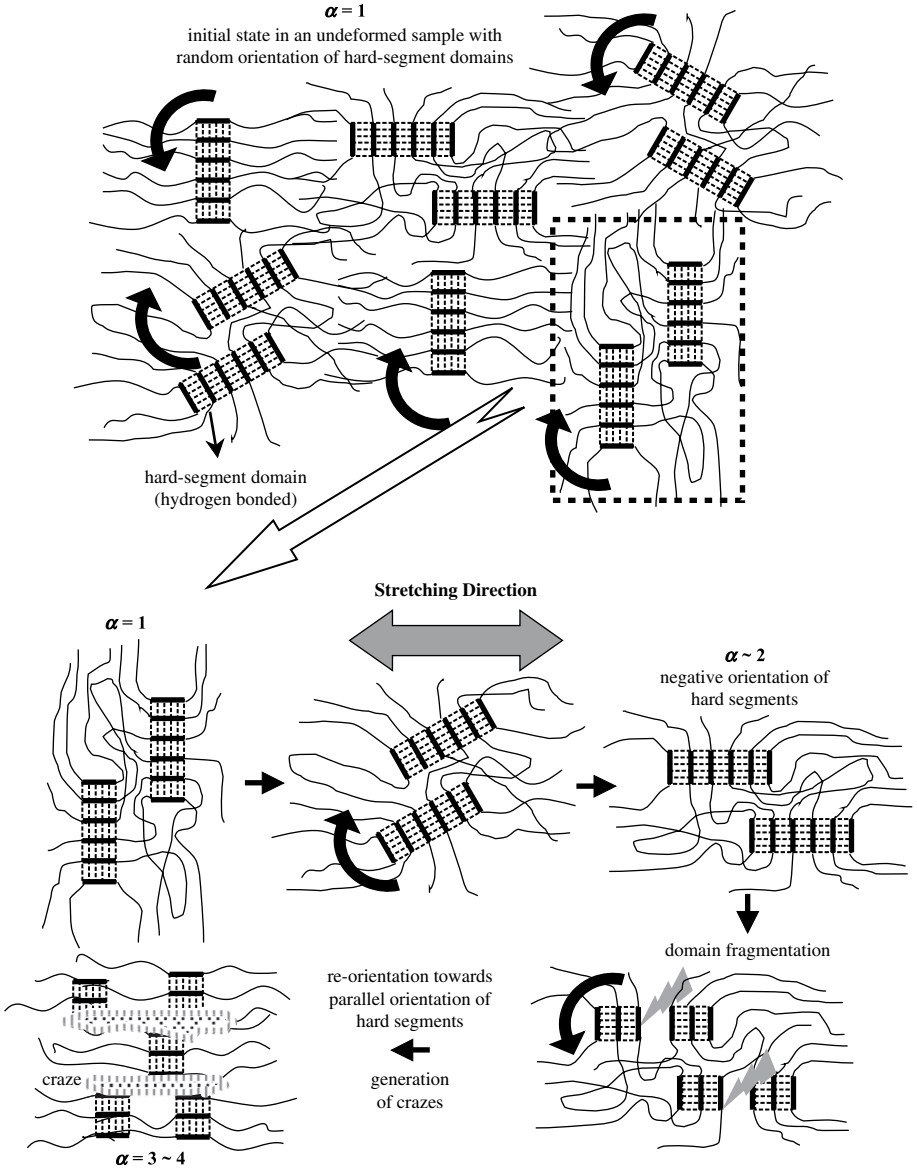

Fig. 1. Schematic illustrations for orientation of the lamellar type hard-segment domains. In the intermediate stage, the hard-segment domain suffers from microscopic fracture so that crazing sets in.

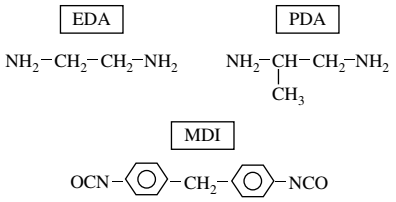

Scheme 1.

PTMG stand for 4,4′-diphenylmethane diisocyanate and poly (tetramethylene glycol), respectively. The number-average molecular weight of the PTMG prepolymer (soft segment) was 1800. Mixture of two different types of chain extenders (diamine compounds), which were ethylenediamine (EDA) and propylenediamine (PDA), was used to control and adjust material property for needs [28]. The chemical formulae for these compounds are shown in Scheme 1. Note here that EDA has high cohesiveness so that the hard-segment domains comprising EDA are firm. However, in the meantime it imparts thixotropy to a solution of EDA-extended polyurethaneurea sample. Since a highly thixotropic solution is not easy to handle, another component PDA is mixed to adjust such a subtle balance of properties. In this study, we used in total four different compositions of EDA/PDA (= 100/0, 80/20, 50/50, 0/100 by weight). Diethyleneamine (DEA) is finally added in the system to terminate the chain extension reaction. Thus, the reaction product (polyurethaneurea) solution in dimethylformamide was obtained. For solution casting, the initial polymer concentration in the cast solution was adjusted to 20% by the amount of DEA added as a terminator. Thickness of the as-cast films was 15 or 70 μm, depending on further measurements for structural analyses.

It should be noted here that chemical reaction between amine and isocyanate groups gives the urethane bonding in polyurethaneurea, while the reaction between two isocyanate groups results in the urea bonding. Therefore, the urea bonding is accommodated always in the hard-segment domains. This fact can be applied to extract information separately for the hard-segment domains by Fourier transformed infrared (FTIR) spectroscopic measurements [5–8,13,16,22–25,28].

2.2. Tensile stress–strain test

Instron Universal Testing Machine 4466 (Instron Co., Ltd.) was used with the fixed stretching rate at 200 mm/min. An approximately 4-mm-wide film with the thickness of 70 μm was clamped with the gauge length of 20 mm. We conducted more than 10 measurements for each polyurethaneurea sample and the most representative stress–strain curve is shown in Fig. 2.

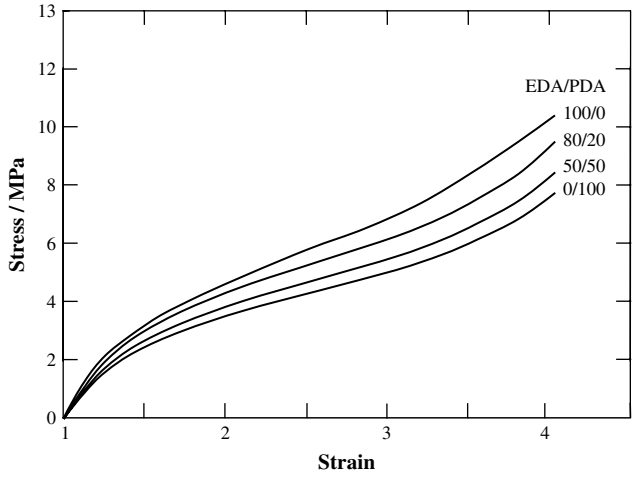

Fig. 2. Stress–strain curves measured at room temperature for polyurethaneurea films with various ratios of EDA/PDA used as a chain extender. The nominal stress is plotted as a function of strain.

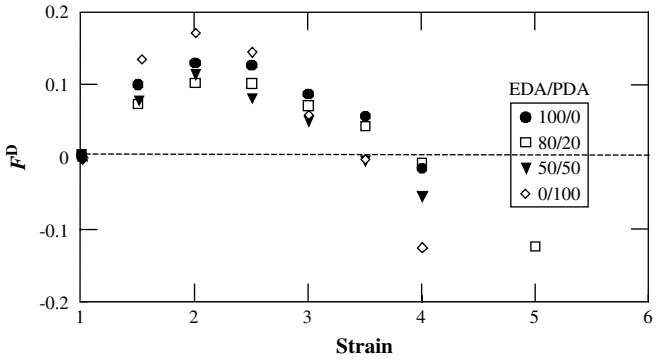

Fig. 3. Plots of dichroic-ratio orientation factor F^D as a function of stretching ratio α. For the evaluation of F^D, the absorption band at 1634 cm^{-1} being ascribed to the stretching vibration of the carbonyl group in hydrogen bonded urea group was used, which was extracted from the FTIR measurements at room temperature.

2.3. FTIR spectroscopic measurements

The orientational behavior of the hard segments under uniaxial stretching provides significant physical insights into resistance and rigidity of hard-segment domains against mechanical deformation. The FTIR spectroscopic measurements allow us to evaluate the orientation factor separately for the hard segments by focusing on the absorption band at 1634 cm^{-1}, which is due to the stretching vibration of the carbonyl group in hydrogen bonded urea group [5,6]. For this purpose, a pair of the spectra along the directions parallel and perpendicular to the uniaxial stretching should be measured. Based on the evaluated dichroic ratio R, we can further evaluate the dichroic-ratio orientation factor F^D.

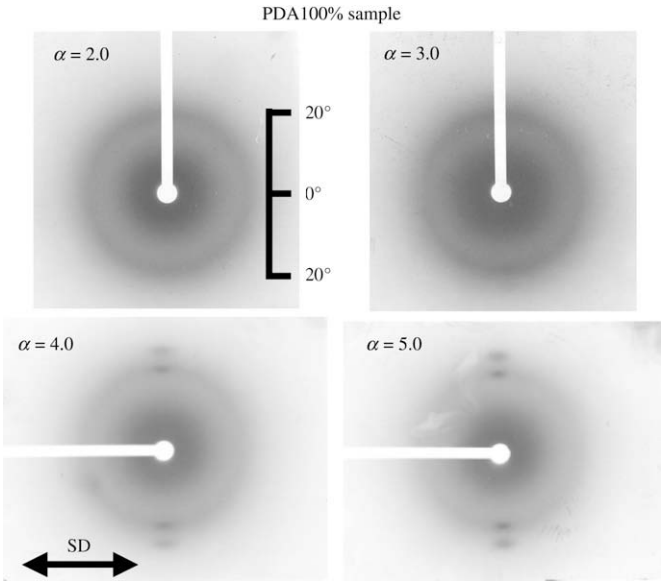

Fig. 4. WAXD patterns measured at room temperature for the PDA100% sample. The stretching direction (SD) is parallel to the equator.

$$F^{D} = (R-1)/(R+2) \quad (1)$$

with

$$R = A_{\parallel}/A_{\perp} \quad (2)$$

where the absorbance A is given by $A = -\ln(I/I_0)$, with I and I_0 being the intensity of the transmitted infrared beam and that of the incident beam, respectively. Because the observed FTIR spectrum comprises several individual absorption peaks overlapping one another, computational peak decomposition was performed to retrieve individual contributions. Then, using absorbance peak at 1634 cm^{-1}, F^{D} is evaluated. Note that in the limit of the dichroic ratio $R \to 0$, the negative orientation factor F^{D} asymptotically approaches to $-1/2$. It is needless to say that this is the case of $A_{\parallel} \to 0$, namely, no absorption in the direction parallel to the stretching direction (SD). This indicates negative orientation of the absorbance transition moment with respect to SD. For the case of $A_{\perp} \to 0$, on the other hand, $R \to \infty$ and hence $F^{D} \to 1$, which is the case of the parallel orientation. Thus, the range F^{D} varies is $-0.5 \le F^{D} \le 1.0$.

We conducted FTIR spectroscopic measurements with step-wise uniaxial stretching with a Spectrum2000 (Perkin Elmer Japan Co., Ltd.) operating at scan number of 16 and a spectral resolution of 4.0 cm^{-1}. The rectangularly prepared films, 30 mm long, 10 mm wide, and 15 μm thick, were subjected to the measurements. During the FTIR measurements the sample was fixed at a given constant length. Right after a pair of the dichroic measurements, which are the spectra along parallel and perpendicular directions to SD, the sample was further stretched for the subsequent FTIR quiescent measurements at the fixed stretching ratio. For more details of the FTIR measurements, refer to some literatures [5–8,13,16,22–25,28].

2.4. Wide-angle X-ray diffraction (WAXD) measurements

As mentioned above, we observed whitening phenomena of the transparent polyurethaneurea film upon the uniaxial stretching from the undeformed state. Stretching-induced crystallization of the soft PTMG segments may be relevant to the whitening phenomena. To detect the stretching-induced crystallization, WAXD measurements were conducted at room temperature with step-wise stretching of the sample (the same protocol as used for the FTIR measurements). We used a conventional X-ray generator RAD2C (Rigaku Corporation) operated at 18 kV–40 mA, which generates the Cu-Kα X-ray with wavelength of 0.154 nm. 2D-WAXD patterns were recorded directly on X-ray-sensitive photographic films with exposure of X-ray for 2 h.

2.5. Optical microscopic (OM) observation

Since the polyurethaneurea film used in this study is transparent at the undeformed state, we may have chance to observe the change in the film appearance along with uniaxial stretching on the optical microscope. Therefore, we performed OM observations with BX50 (OLYMPUS) microscope at room temperature with step-wise

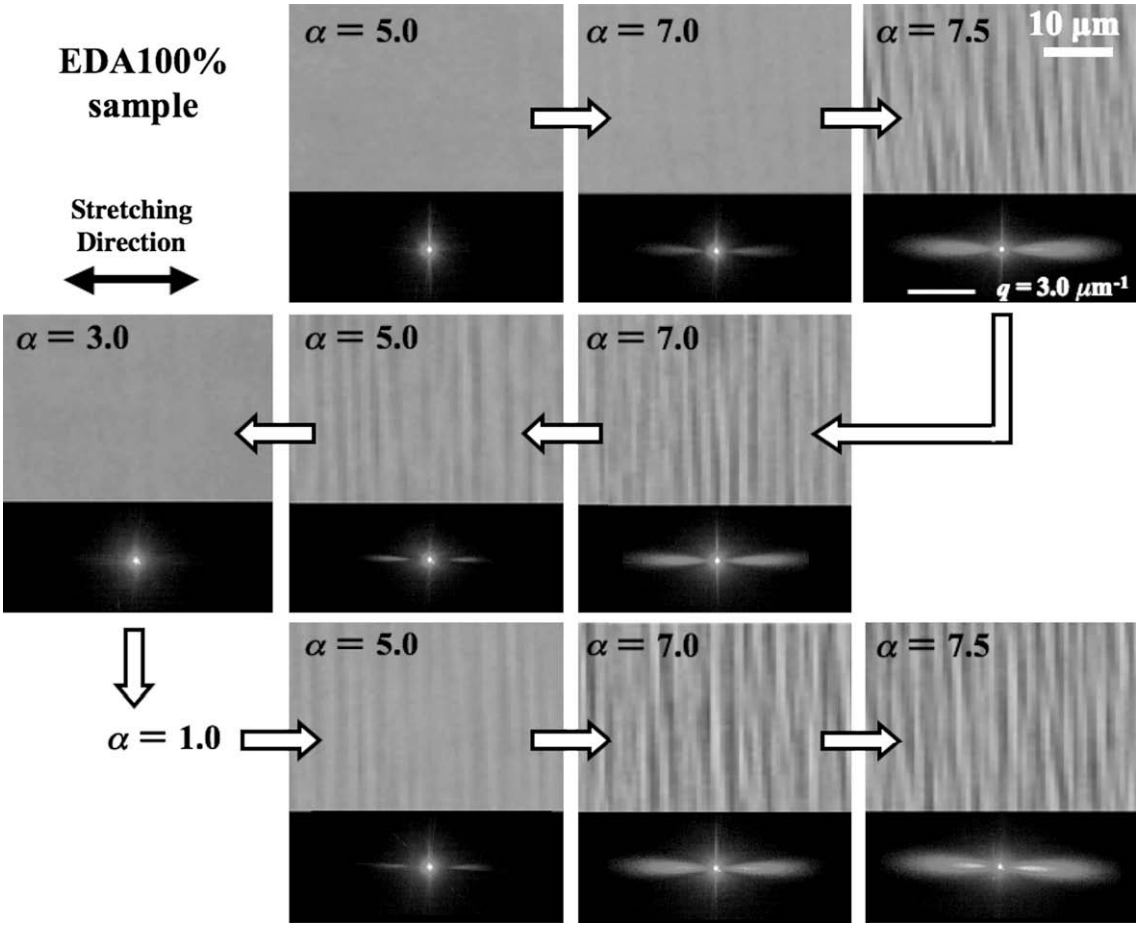

Fig. 5. Optical microscopic images observed at room temperature together with corresponding 2D Vv-SALS patterns for the EDA100% sample in the stretching process (so-called the first run) as well as those in the reversed process by removing the stress and in the re-stretching process (so-called the second run). The stretching direction (SD) is horizontal.

stretching of the sample under the microscope (the same protocol as used for the FTIR measurements). The observed images were recorded directly on photographic films.

2.6. Two-dimensional (2D) Vv-SALS measurements

To obtain more quantitative results complementary to the OM observations, 2D Vv-SALS patterns were measured at room temperature with step-wise stretching of the sample (the same protocol as used for the FTIR measurements). A He–Ne laser with the wavelength of 632.8 nm and the beam size of 1.5 mm was used as a light source. The observed 2D Vv-SALS patterns were recorded directly on photographic films. The sample-to-detector (screen) distance was 115 mm.

2.7. 2D-USAXS measurements

The 2D-USAXS experiments were performed at the 'medium-length beamline' BL20XU, SPring-8 (Hyogo, Japan) at room temperature with step-wise stretching of the sample (the same protocol as used for the FTIR measurements). Namely, we simply performed the 2D-USAXS measurements one by one with holding the sample at fixed stretching ratio, followed by subsequent extension to the next destination of stretching ratio. The BL20XU is an undulator beamline bearing two experimental hutches apart each other by approximately 150 m. An evacuated flight path with an inner diameter of 10 cm is placed to connect the two hutches. Several pieces of Kapton films were used as window materials for the evacuated flight path. A sample was set in the first hutch and a scattering pattern is recorded in the second hutch using a cooled charge-coupled device (CCD) detector (C4880, Hamamatsu Photonics Ltd.) equipped with an X-ray image intensifier (V7339P, Hamamatsu Photonics Ltd., XRII). The exposure time was 10 s. The sample-to-detector distance was 160.5 m and the incident X-ray energy was 23 keV, corresponding to the wavelength of 0.0539 nm. More details of the USAXS beamline are described in literatures [26,27].

3. Results and discussion

Fig. 2 shows the stress–strain curves at room temperature for all of the samples used in this study. Note that the nominal stress is plotted as a function of strain. As described above, these samples differ in the ratio of EDA/PDA, chain extenders. Due to the strong cohesive interaction between the EDA moieties, it can be clearly confirmed in Fig. 2 that the stress level is higher for the sample with the higher EDA content.

The dichroic-ratio orientation factor F^D, which was evaluated using the absorption band at 1634 cm^{-1} being ascribed to the stretching vibration of the carbonyl group in hydrogen bonded urea group is plotted as a function of stretching ratio α in Fig. 3. It is clearly seen that F^D increases with stretching up to $\alpha = 2$. Then the behavior turned into opposite one via the maximum of F^D, being continuously decreased. Finally, the value of F^D changed into

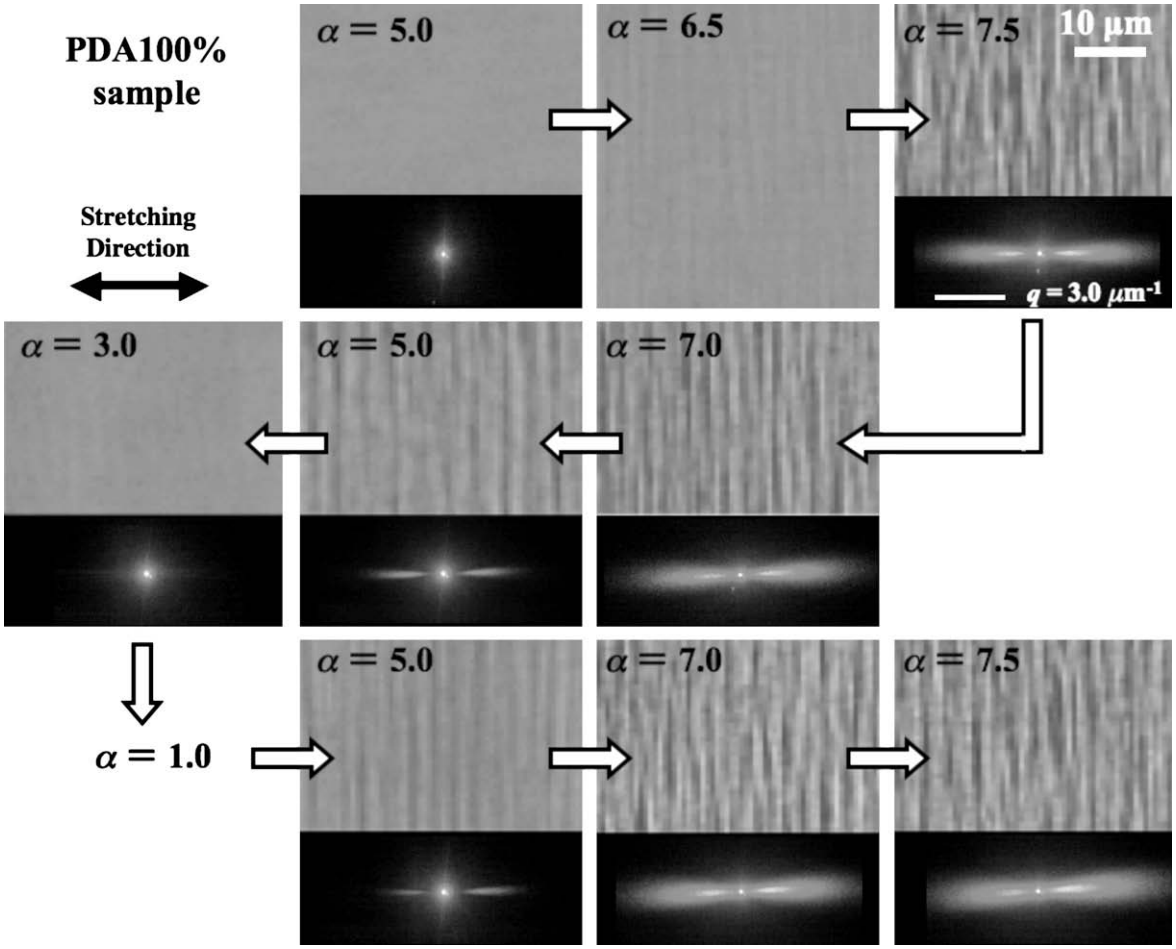

Fig. 6. Optical microscopic images observed at room temperature together with corresponding 2D Vv-SALS patterns for the PDA100% sample in the stretching process (so-called the first run) as well as those in the reversed process by removing the stress and in the re-stretching process (so-called the second run). The stretching direction (SD) is horizontal.

negative one around $\alpha = 3.5$–4.0, of which order roughly depends on the EDA/PDA ratio, for which we will discuss later.

To understand the behavior of F^D, the following fact should be taken into account. The transition moment of the stretching vibration of the carbonyl group, we are now focusing on, is approximately perpendicular to the hard segments in the main chain of polyurethaneurea, so that the negative orientation factor F^D definitely indicates positive orientation of the hard segments and in turn that of the polymer main chain, and vice versa. Thus, the hard segments first orients perpendicular to SD in the early stage of the stretching (for $\alpha \leq 2.0$) and then turned into the parallel orientation for $\alpha \geq 2.0$. This kind of behavior has been well known [5,6,22–25,28]. One of the most reasonable explanations of this result is as follows. In the early stage, the hard-segment domains are to be oriented as a whole. If the lamellar shape can be assumed for the domain, as shown in Fig. 1, then the longer axis of the lamellar domain should be oriented parallel to SD. This further suggests that the hard segments exhibit the negative orientation, bearing in mind that the hard segments embedded in the lamellar domain are perpendicular to its longer axis. Subsequent stretching causes localized plastic fracture of the hard-segment domains and therefore the larger domains should undergo fragmentation, giving rise to reduction in anisotropy of the hard-segment domain shape. Therefore, the negative orientation of the hard segment will be decelerated. Such a structural change is schematically shown in Fig. 1. It is interesting to point out in Fig. 3 that the maximum of F^D seems to shift towards higher stretching ratio with an increase of the EDA content. Furthermore, similar tendency may be found for the behavior of the intercept of the abscissa where $F^D = 0$. Both can be rationalized to the higher cohesiveness due to EDA. Although there are discernible differences in the behaviors of these samples, all of them are substantially identical to each other. In conclusion, the samples suffer from plastic fracture even in an early stage of stretching (around $\alpha = 2.0$), much earlier than $\alpha = 6.5$ where typically the whitening phenomena were observed. Note here that even in this case the sample recovered transparency when the stress was removed. This fact suggests that the deformation is not permanent.

Fig. 4 displays the WAXD results for the PDA100% sample. SD is parallel to the equator. Only the amorphous halo was detected below $\alpha = 3.0$, whereas two pairs of reflection due to the crystallization of the soft PTMG segments were definitely seen above $\alpha = 4.0$. Bearing in mind that the whitening occurred at approximately $\alpha = 6$–7, it seems that the strain-induced crystallization of PTMG does not result in the whitening of the film. Thus, we further explored structural changes responsible for the whitening.

Figs. 5 and 6 show results of OM observations together with corresponding 2D Vv-SALS patterns for the EDA100% sample and for the PDA100% sample, respectively. Figs. 5 and 6 contain results

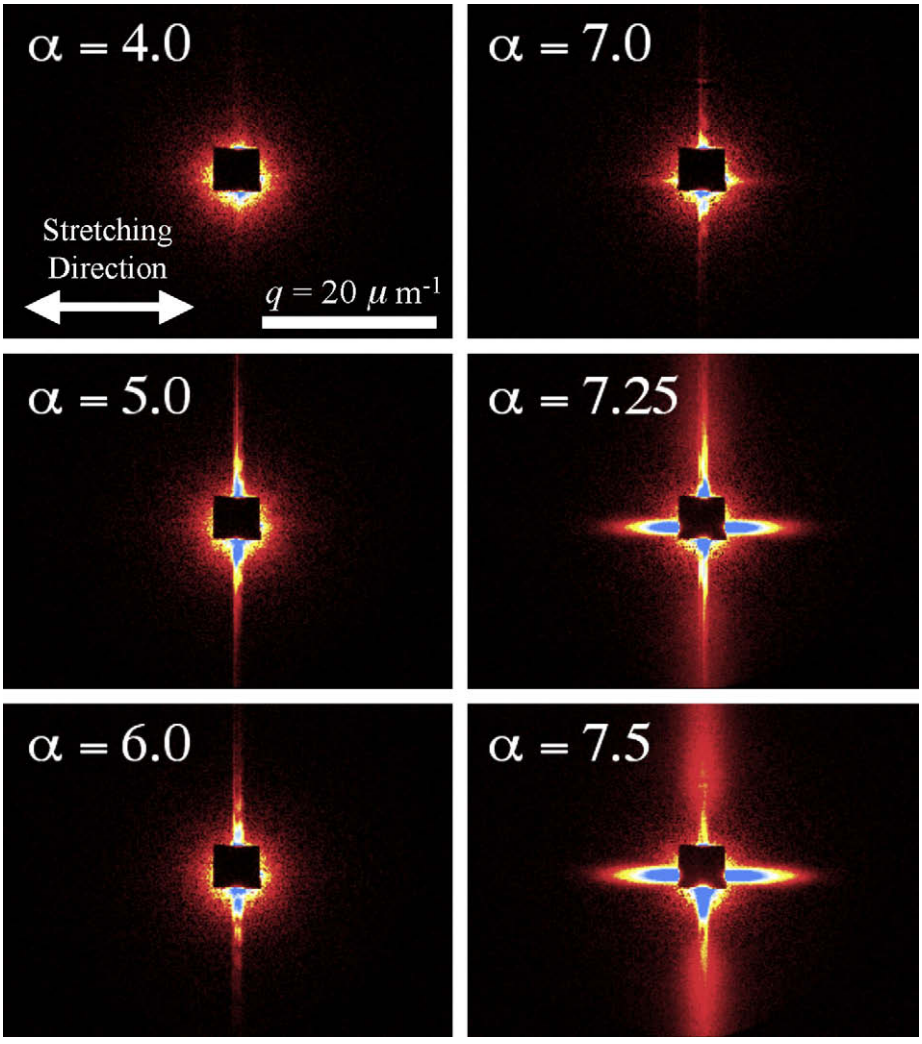

Fig. 7. 2D-USAXS patterns measured at room temperature for the PDA100% sample. The stretching direction (SD) is parallel to the equator.

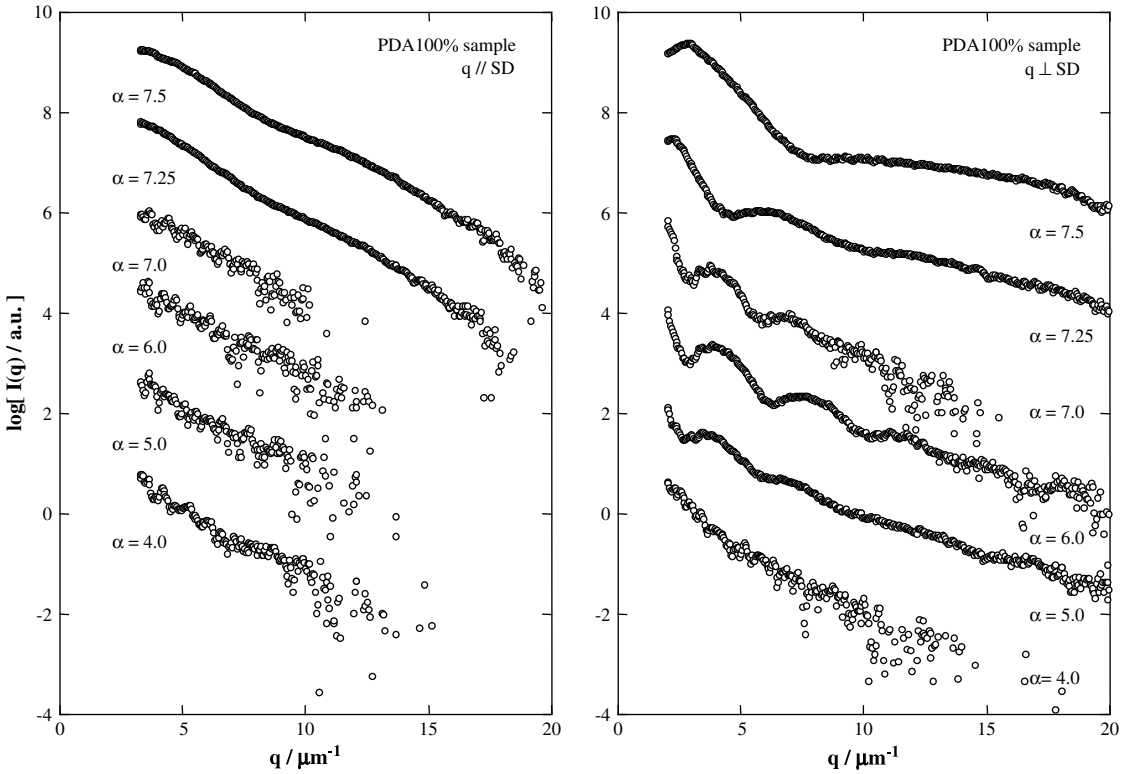

Fig. 8. One-dimensional scattering profiles for the PDA100% sample, the scattering intensity $I(q)$ vs. the scattering vector $\boldsymbol{q}$, for (a) $\boldsymbol{q} \parallel$ SD and (b) $\boldsymbol{q} \perp$ SD. The profiles were obtained from 2D-USAXS patterns by conducting sector average.

obtained in the stretching process (so-called the first run) as well as those in the reversed process by removing the stress and those in the re-stretching process (so-called the second run). Here, SD is horizontal. Overall, we observed formation of periodically alternating and space-filling stripes which are almost perpendicular to SD in the OM images. The onset of the formation was found at $\alpha = 7.0$ for the EDA100% sample, while it was at $\alpha = 6.5$ for the PDA100% sample. Although the appearance in the OM photo was

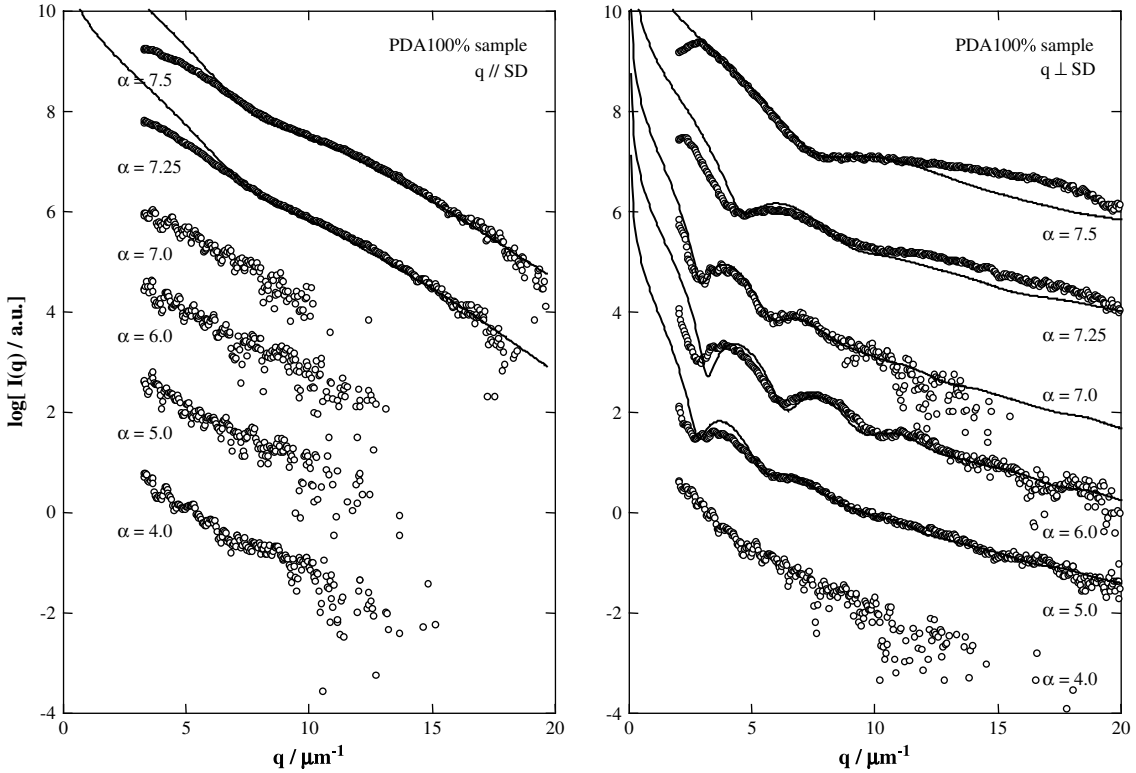

Fig. 9. Results of the model calculation to be fitted to the experimental data (the same SAXS profiles as shown in Fig. 8).

ambiguous, the corresponding 2D Vv-SALS pattern was more reliable as it was clearly exhibiting strong streaks in the direction parallel to SD. The streak is a signature of stripes perpendicular to SD. Then a question will be raised, what are the stripes ascribed to? To answer this question, the OM observation was conducted in the reversed process by removing the stress. As shown in Figs. 5 and 6, the stripes completely disappeared for both samples upon the release of the stress at $\alpha = 3.0$. This suggests that the stripes are not permanent. It is further interesting to find that the stripes appear much earlier in the second run of the stretching, as is clearly confirmed in Figs. 5 and 6. This hysteresis, on the other hand, implies that there would be a permanent damage in the highly stretched sample during the first run, although its appearance is transparent. Overall, the stripe formation can be considered as a transient phenomenon but permanent damage in the microscopic structures remains, which would be referred to as micro-cracking. To further detect the microscopic formation of crazes and cracks, we conducted the USAXS measurements. At this moment, it is interesting to point out that there is a trivial difference between the behaviors for the EDA100% and the PDA100% samples observed in Figs. 5 and 6, respectively. Especially, the onset value of α at which the stripes became discernible is a bit retarded for the EDA100% sample, being attributed to the higher cohesiveness of EDA, as compared to the PDA100% sample.

We have to pay attentions to evolution of the cross streaks which are perpendicular to SD for the EDA100% sample, although the intensity is much weaker as compared to those parallel to SD. Nevertheless, we should be aware of the fact that the evolution of the streaks perpendicular to SD preceded those parallel to SD at $\alpha = 5.0$ in Fig. 5 where no streak appeared in the direction parallel to SD. Another important finding in the Vv-SALS results is existence of a peak on the streak parallel to SD. From the position of the peak we were able to calculate spacing 4.19 μm at $\alpha = 7.5$ for the PDA100% sample, which was in good agreement with the separation between the periodically alternating stripes observed in the OM pictures. We will discuss this fact later in relation with the USAXS results.

We are now in a position to examine the results of 2D-USAXS. Fig. 7 shows the 2D-USAXS patterns as a function of α for the PDA100% sample. For the deformed film, SD is parallel to the equator. Up to $\alpha = 4.0$, no change in the pattern was observed. At $\alpha = 5.0$ the meridional streaks, which are perpendicular to SD, became intense. Bearing in mind that the corresponding 2D Vv-SALS pattern displayed streaks in the direction perpendicular to SD at $\alpha = 5.0$ [29], the appearance of the meridional streaks in the 2D-USAXS pattern can be ascribed to the same structural change. As for the equatorial streaks parallel to SD, they became discernible at $\alpha = 7.0$, which shows good correlation with the evolution of the stripes in the OM photo at $\alpha = 6.5$. Thus, the 2D-USAXS pattern finally showed the bright cross streaks both in the directions parallel and perpendicular to SD above $\alpha = 7.0$.

For the quantitative analyses, one-dimensional scattering profiles, the scattering intensity $I(q)$ vs. the scattering vector $\boldsymbol{q}$, were extracted from the 2D-USAXS pattern in the direction of $\boldsymbol{q} \parallel$ SD and $\boldsymbol{q} \perp$ SD by conducting sector average. Here, the magnitude of $\boldsymbol{q}$ is given as:

$$|\boldsymbol{q}| = (4\pi/\lambda)\sin(\theta/2) \tag{3}$$

with λ and θ being the wavelength of the incident X-ray and the scattering angle, respectively. Fig. 8 shows the results. As mentioned above, the excess scattering was not discernible up to $\alpha = 7.25$ for $\boldsymbol{q} \parallel$ SD and up to $\alpha = 5.0$ for $\boldsymbol{q} \perp$ SD. The most surprising fact is that interference appeared upon the uniaxial stretching in the USAXS profile with $\boldsymbol{q} \perp$ SD especially in a range of $5.0 \leq \alpha \leq 7.5$. Such interference is generally ascribed to spatial order or particles with nearly uniform size, which might suggest the generation of scatterers with micron size in the film being uniaxially stretched. It is needless to state that polyurethaneureas form nano-structures, but in the micrometer scale it is uniform. Therefore, the generation of scatterers with micron size is quite striking.

Model calculation of the scattering intensity enables us to figure out the shape of the scatterers evolved. We found that calculation with assuming lamellar shape can reproduce the experimentally obtained USAXS profiles much better as compared to the case assuming spherical or cylindrical shape. The results of the calculation to be fitted to the experimental data are shown by the solid curves in Fig. 9. For the calculation, we used the following equation for the lamellar particle with thickness of L [30,31]:

$$I(q) \sim \left\langle f^2 \right\rangle / q^2 \tag{4}$$

$$f = \{[\sin(qL/2)/(qL/2)]\}\exp\left(-\sigma^2 q^2/2\right) \tag{5}$$

Here, the so-called Lorentz factor (q^{-2}) is included in Eq. (4) in order to correct for distribution in orientation of the lamellar particles. Furthermore, the finite thickness of the interface is taken into account. Actually, the parameter σ in Eq. (5) characterizes it and rationalizes the characteristic thickness of the interface, t_l, through the following relationship:

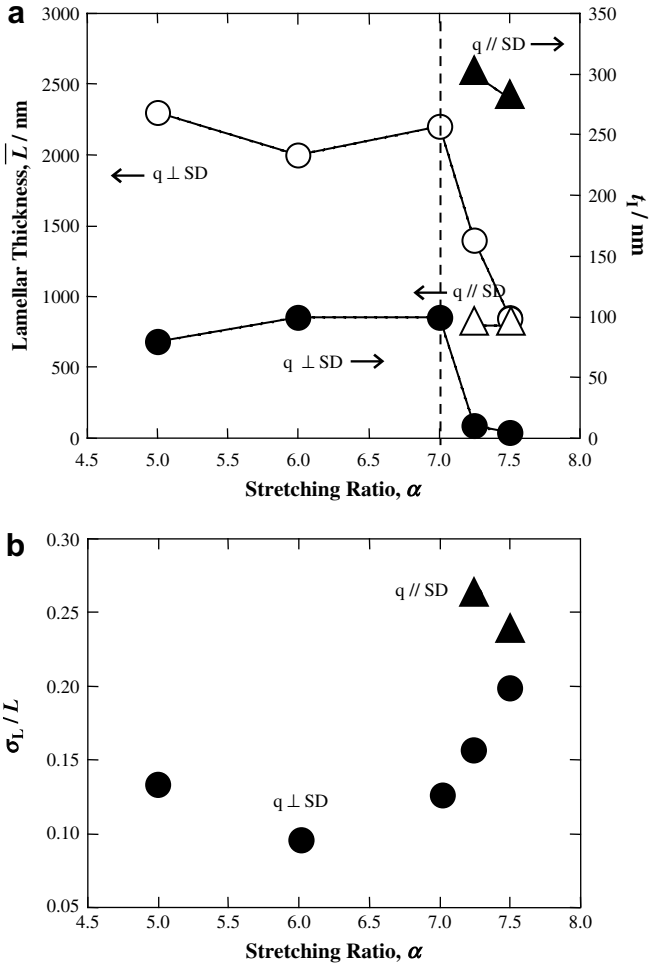

Fig. 10. (a) Plots of average thickness of lamellar-shaped crazes $\bar{L}$ and the standard deviation of the thickness distribution σ_L as a function of the stretching ratio α. (b) Plot of normalized standard deviation of the thickness distribution $\sigma_L/\bar{L}$ as a function of the stretching ratio α.

$$t_I = (2\pi)^{1/2}\sigma \quad (6)$$

The size distribution for the lamellar particles is also incorporated in the calculation to take average of f^2 in Eq. (4). Actually, the Gaussian distribution function $P(L)$ is assumed:

$$P(L) = \left(2\pi\sigma_L^2\right)^{-0.5} \exp\left[-(L-\bar{L})^2/2\sigma_L^2\right] \quad (7)$$

where L is the thickness of a lamellar particle and $\bar{L}$ is its average, and σ_L denotes the standard deviation for the thickness distribution. Thus, we can calculate the scattering function by adjusting the structural parameters. As shown in Fig. 9, the model calculation approximately accounts for the experimental results, which in turn suggests generation of lamellar-shaped scatterers in the stretched film. As we observed whitening at approximately $\alpha = 6.5$, it is reasonable to consider that the scatterers are crazes. Moreover, their shape is lamellar. This is only a possible outcome of the 2D-USAXS measurements so that further experimental examination of the shape should be needed. It was further found that the 1D-USAXS profile is almost featureless along the scattering vector which is not parallel to equator, or meridian. This indicates that the lamellar scatterers are highly oriented either parallel or perpendicular to SD. Note here that the interference peaks appeared at $\alpha = 5.0$ in the profile for $\boldsymbol{q} \perp$ SD, which precedes the whitening of the film but is in very good accord with appearance of the meridional streaks in the Vv-SALS pattern at $\alpha = 5.0$. Considering the deficiency of the SALS technique for quantitative analyses of the meridional streaks, the appearance of the several interference peaks in the meridional streaks in the 2D-USAXS pattern definitely indicates high potential and benefits of the USAXS technique for microscopic studies of material fracture.

The best fit to the experimental data enables us to evaluate the values for the structural parameters, $\bar{L}$, σ_L and t_I. Among them, $\bar{L}$ and t_I are shown in Fig. 10(a) as a function of the stretching ratio. Note that t_I is much larger for $\boldsymbol{q} \parallel$ SD and the fraction of the interfacial thickness is 35% or more. However, this is not so amazing. In the model for the calculation of the particle scattering function, the one-dimensional profile of the electron density distribution for the diffuse interface is approximated to be hyperbolic tangent-type function (actually which is more approximated by taking the convolution of a step function with the Gaussian function). Furthermore, the characteristic thickness of interface (t_I) is resulted by linear approximation of the slope of the hyperbolic tangent function for the diffuse interface (see Fig. 11(e) for the definition of t_I). Therefore, the one-dimensional profile of the electron density distribution is slightly changing up to about twice of t_I towards the interior of the lamellar particle. In other words, the one-dimensional profile of the electron density distribution can be considered to be constant at the central portion of the lamellar particle with the thickness of about $\bar{L} - 2t_I$. If the characteristic thickness is less than 50% of $\bar{L}$, this means that the core of the

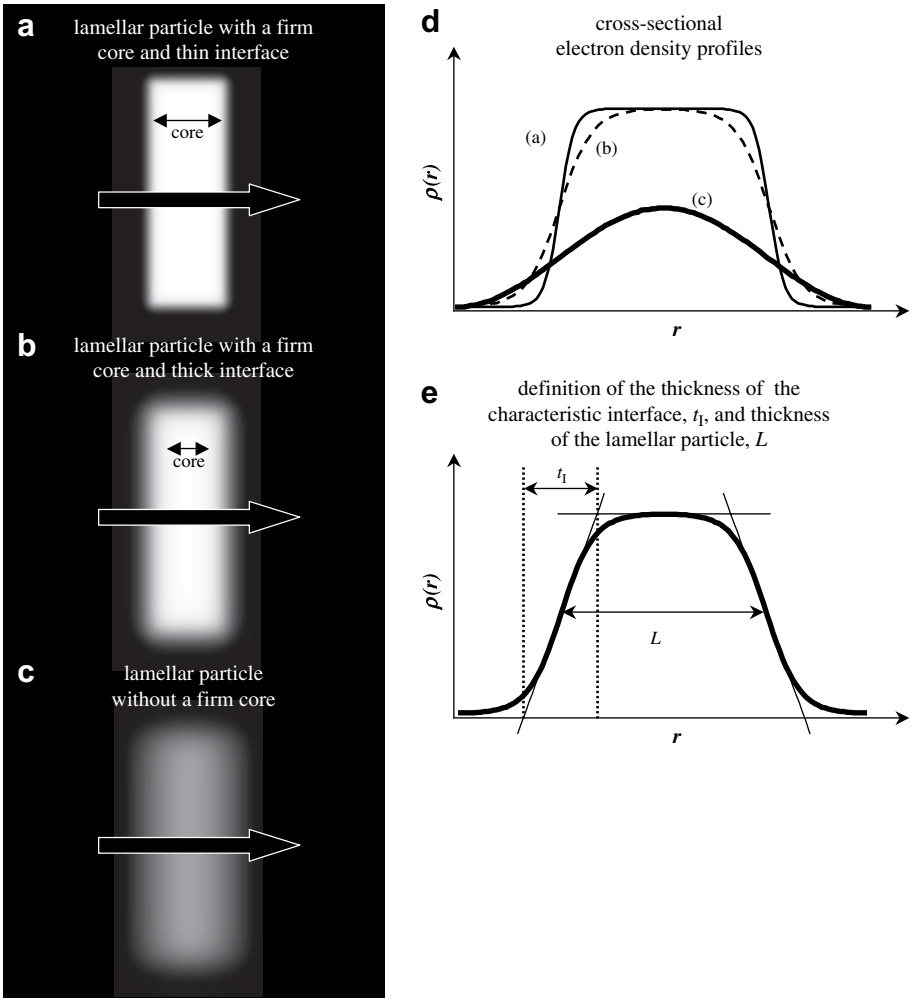

Fig. 11. Schematic illustrations for the physical picture of various types of lamellar particles; (a) lamellar particle with a firm core and thin interface, (b) lamellar particle with a firm core and thick interface, and (c) lamellar particle without a firm core. (d) The cross-sectional electron density profiles, $\rho(r)$, along the horizontal thick arrows in the respective pictures of parts (a)–(c). (e) The definition of the thickness of the characteristic interface, t_I, and thickness of the lamellar particle, L.

lamellar particle (zone excluding the interfacial regions) is enough firm (see Fig. 11(b)). On the other hand, when the characteristic thickness is greater than 50% of $\bar{L}$, it is of course nonsense. Refer to Fig. 11(a)–(d) for the physical picture of various types of lamellar particles; (a) lamellar particle with a firm core and thin interface, (b) lamellar particle with a firm core and thick interface, and (c) lamellar particle without a firm core, as well as (d) the cross-sectional electron density profiles, $\rho(r)$, along the horizontal thick arrows in the respective pictures of Fig. 11(a)–(c).

In the early and intermediate stages of the stretching ($\alpha \leq 7.0$), the interference peaks appear only for $\boldsymbol{q} \perp$ SD and resultant $\bar{L}$ exhibits almost constant within the range of 2.0–2.3 μm. At $\alpha = 7.25$, there observed a discrete decrease in $\bar{L}$, down to about 1.3 μm. In accordance with this change, the interference became discernible in the profile for $\boldsymbol{q} \parallel$ SD, from which the value of $\bar{L}$ is evaluated as approximately 0.8 μm (which is discernible in optical micrographs in Fig. 6 and the onset of its formation is around $\alpha = 6.5$, being also consistent with each other). As for the characteristic thickness of interface t_I, similar phenomenon is observed for $\boldsymbol{q} \perp$ SD, i.e., there is a discrete decrease in t_I at $\alpha = 7.25$. The change from broad to sharp interface reminds us occurrence of a permanent damage, although at this moment, we have no concrete idea to specify what kind of structural change it is. However, one of the possible models accompanies irreversible process from craze to micro-cracks (permanent damages) upon stretching further than $\alpha = 7$. This further implies fibrillization within a craze (see Fig. 12). Such kind of transformation from craze to micro-cracks may be responsible for the sudden decrease in $\bar{L}$ around $\alpha = 7.25$ and for hysteresis observed in Figs. 5 and 6 (*plastic feature* of this material). The reason why the transformation from craze to micro-cracks takes place all at once over the sample around $\alpha = 7.25$ may be considered as follows. The activation energy for the fibrillization sets a criterion in the stress level. When the stress is below it, crazes are stable with no transformation into micro-cracks. As the stress increases, the number of crazes would be increased but the thickness of crazes remains constant. When the stress reaches the critical value, the fibrillization sets in, giving rise to sharp interface and micro-cracks, which in turn results in the sudden decrease in $\bar{L}$. Comparing the PDA100% sample with the EDA100% sample, the former one should have a slightly lower critical value of the stretching ratio α, because of the lower cohesive energy. This is already confirmed by the optical microscopic observation shown in Figs. 5 and 6, which in turn confirms the speculation why structural changes suddenly occurred at a given degree of stretching. Fig. 10(b) shows the normalized standard deviation $\sigma_L/\bar{L}$, exhibiting a steep increase for $\alpha \geq 7.0$. Since the generation of the scatterers is attributed to fracture (micro-cracking), the size distribution becomes broader.

On the contrary, t_I is much larger for $\boldsymbol{q} \parallel$ SD. This means that the newly evolved lamellar-shaped crazes, which are perpendicular to SD and periodically ordered in SD (observed in Fig. 6), have very diffuse interface. Bearing in mind that the thickness of the crazes is about 0.8 μm, the fraction of the interfacial thickness is 35% or more (see Fig. 11(b)). Since these crazes are not rigid but diffuse so that they are considered to be responsible for elastomeric feature of this material, i.e., the whitening completely disappears when the stress is removed (*elastomeric feature* of this material).

Based on the structural analyses, we finally provide a possible model for the process of fracture upon the uniaxial stretching of the polyurethaneurea film (the PDA100% sample) in Fig. 13. Below the stretching ratio of 7.0, the meridional streaks appear in $\boldsymbol{q} \perp$ SD, which means that the lamellar-shaped crazes are generated parallel to SD. Unfortunately, it was impossible to figure out the lateral size of them, their thickness was found to be uniform in the range of 2.0–2.3 μm. As schematically shown in Fig. 1, the lamellar crazes are generated parallel to SD as a consequence of shear deformation

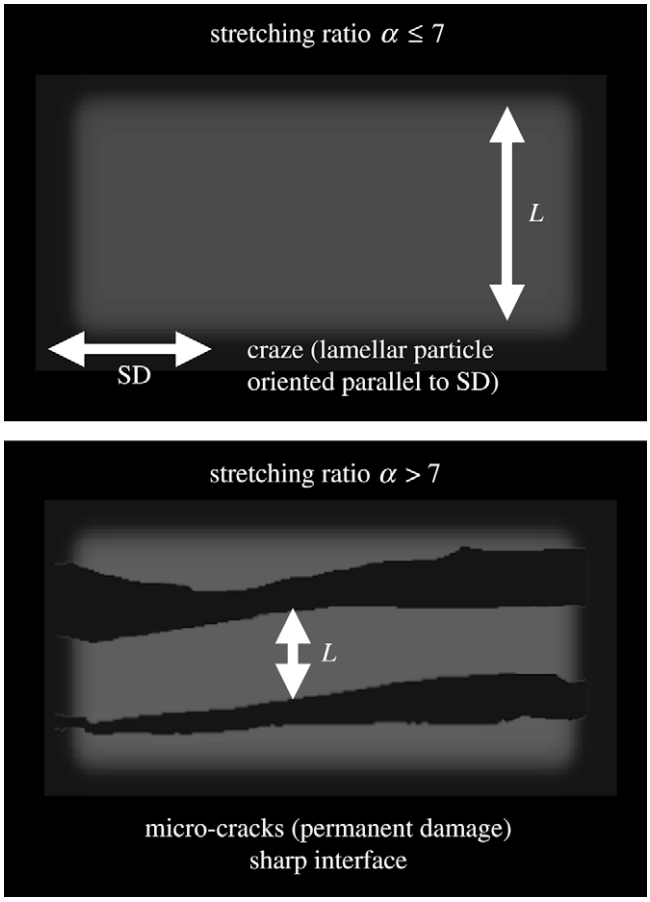

Fig. 12. Schematic explanation for the sudden decreases at $\alpha = 7$ in the interfacial thickness and the thickness of lamellar particles, which are oriented parallel to the stretching direction. Here, irreversible process from craze to micro-cracks (permanent damages) upon stretching further than $\alpha = 7$ is suggested.

induced localized fracture within a lamellar hard-segment domain, which is so oriented that the hard segments are parallel to SD, as is confirmed by the negative value of F^D above $\alpha = 5.0$ in Fig. 3.

On the other hand, their thickness decreased dramatically down to approximately 0.8 μm above the stretching ratio of 7.25, where the film was turned to be turbid. This may be due to shear thinning. Furthermore, the interfacial thickness also discretely decreased. This implies the lamellar-shaped micro-cracks parallel to SD may be responsible for *plastic feature* of this material. In the meantime, lamellar-shaped crazes newly evolved perpendicular to SD, with their thickness of about 0.8 μm. The interfacial thickness for these crazes was found quite diffuse. This implies the lamellar-shaped crazes perpendicular to SD may be responsible for *elastomeric feature* of this material. Although similar values of thickness were found for the lamellar-shaped crazes aligned parallel and perpendicular to SD, we should sate at this moment that the agreement of the thickness might be accidental because we have no idea about dynamic interplay between the two directions parallel and perpendicular to SD. Finally, it is quite curious to find that lamellar-shaped crazes newly evolved perpendicular to SD were ordered regularly by separation of 4.19 μm. Such an ordering phenomenon reminds us nonlinear pattern formation. As a matter of fact, the uniaxial stretching of film can produce regularly ordered stripes perpendicular to SD, as Toda et al. [32] have reported self-excited oscillation in the neck propagation in amorphous poly(ethylene terephthalate) film. However, this is the case of permanent damages remained as whitening (necking) so that it is quite contrast to the phenomenon reported in the current paper, which is

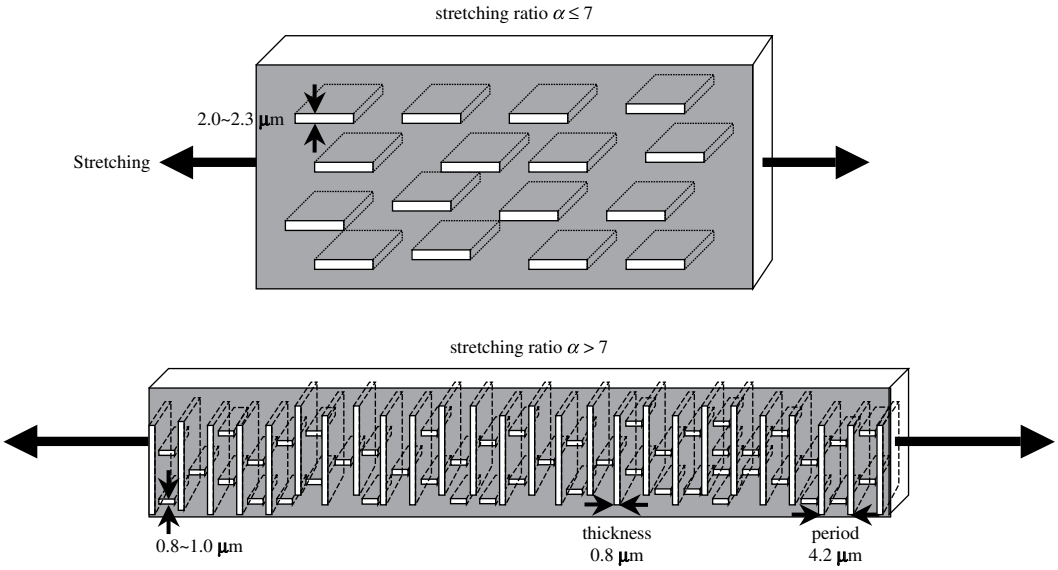

Fig. 13. Schematic illustrations of a possible model for the process of fracture upon the uniaxial stretching of the polyurethaneurea film (the PDA100% sample), which is constructed based on the results of 2D-USAXS.

totally elastic such that the strain could be almost removed and the whitening disappeared. Therefore, the mechanism may be completely different, on which the study deserves a future work.

4. Conclusion

OM observations, 2D Vv-SALS, and 2D-USAXS were conducted to reveal the process of fracture upon the uniaxial stretching of the polyurethaneurea film. It was found that these techniques could cover individual size scales with sufficient overlaps and therefore we could analyze structures in a considerably wide range of size. Actually in this study, the q ranges covered by SALS as $0.5 \leq q \leq 5\ \mu m^{-1}$ and by USAXS as $3 \leq q \leq 20\ \mu m^{-1}$ have an overlap with $3 \leq q \leq 5\ \mu m^{-1}$ which allow us to adjust commensuration of SALS and USAXS scattering curves to obtain a wide-range scattering function in total $0.5 \leq q \leq 20\ \mu m^{-1}$. Although the conventional SAXS was not used here, combination of all will provide $0.5 \times 10^{-3} \leq q \leq 1.5\ nm^{-1}$, hopefully without intermittence. A possible model for the process of fracture was constructed based on the experimental results and is given in Fig. 13. Unfortunately, this is totally static. Dynamic aspect should be studied for understanding of the whole process of fracture, which requires challenging time-resolved USAXS measurements in microseconds.

Acknowledgement

This work is supported in part by the Grant-in-Aid for Scientific Research on Priority Area "Soft Matter Physics" from the Japanese Ministry of Education, Culture, Science and Sport (19031015 granted to SS). The 2D-USAXS experiments were performed at SPring-8 (approval number 2005A0690-NL2b-np). We thank technical supports for the 2D-USAXS experiments from Drs. N. Yagi, Y. Suzuki and K. Uesugi at SPring-8.

References

[1] Cooper SL, Tobolsky AV. J Appl Polym Sci 1996;10:1837.
[2] Bonart R. J Macromol Sci Phys 1968;B2:115.
[3] Bonart R, Morbitzer L, Hentze G. J Macromol Sci Phys 1969;B3:337.
[4] Bonart R, Morbitzer L, Muller EH. J Macromol Sci Phys 1974;B9:447.
[5] Ishihara H, Kimura I, Saito K, Ono H. J Macromol Sci Phys 1974;B10:591.
[6] Kimura I, Ishihara H, Ono H, Yoshihara N, Nomura S, Kawai H. Macromolecules 1974;7:355.
[7] Ishihara H, Kimura I, Yoshihara N. J Macromol Sci Phys 1983–84;B22:713.
[8] Kotani T, Hayashi H, Ishihara H, Matsui T. J Macromol Sci Phys 1992;B31:65.
[9] Jun H-W, West JL. J Biomed Mater Res Part B Appl Biomater 2005;72B:131.
[10] Jun H-W, West JL. J Biomater Sci Polym Ed 2004;15:73.
[11] Guan J, Wagner WR. Biomacromolecules 2005;6:2833.
[12] Demir MM, Yilgor I, Yilgor E, Erman B. Polymer 2002;43:3303.
[13] Shibayama M, Suetsugu M, Sakurai S, Yamamoto T, Nomura S. Macromolecules 1991;24:6254.
[14] Sakurai S, Nokuwa S, Morimoto M, Shibayama M, Nomura S. Polymer 1994;35:532.
[15] Lee HS, Yoo SR, Seo SW. J Polym Sci Part B Polym Phys 1999;37:3233.
[16] Sakurai S, Okamoto Y, Sakaue H, Nakamura T, Banda L, Nomura S. J Polym Sci Part B Polym Phys 2000;38:1716.
[17] Jimenez G, Asai S, Shishido A, Sumita M. Eur Polym J 2000;36:2039.
[18] Klinedinsta DB, Yilgörb E, Yilgörb I, Beyerc FL, Wilkes GL. Polymer 2005;46:10191.
[19] Yeh F, Hsiao BS, Sauer BB, Michel S, Siesler HW. Macromolecules 2003;36:1940.
[20] Blundell DJ, Eeckhaut G, Fuller W, Mahendrasingam A, Martin C. Polymer 2002;43:5197.
[21] Blundell DJ, Eeckhaut G, Fuller W, Mahendrasingam A, Martin C. J Macromol Sci Phys 2004;B43:125.
[22] Shibayama M, Kawauchi T, Kotani T, Nomura S, Matsuda T. Polym J 1986;18:719.
[23] Shibayama M, Ohki Y, Kotani T, Nomura S. Polym J 1987;19:1067.
[24] Yamamoto T, Shibayama M, Nomura S. Polym J 1989;21:895.
[25] Yamamoto T, Shibayama M, Nomura S. Polym J 1991;23:311.
[26] Yagi N, Inoue K. J Appl Crystallogr 2003;36:783.
[27] Shinohara Y, Kishimoto H, Inoue K, Suzuki Y, Takeuchi A, Uesugi K, et al. J Appl Crystallogr 2007;40:s397.
[28] Hashimoto F, Shibaya M, Ishihara H, Ohara T, Iwasaka H, Ota Y. J Textile Eng 2006;52:131 (in Japanese).
[29] Note that this is the result for the EDA100% sample and such a streak was not discernible in the 2D Vv-SALS patterns for the PDA100% sample. However, we consider that these unfavorable results may be due to experimental error and it should be possible to obtain similar results even for the PDA100% sample, because Yoshihara et al. successfully observed the OM image with cross-hutched stripes for the PDA100% sample (unpublished results).
[30] Shibayama M, Hashimto T. Macromolecules 1986;19:740.
[31] Sakurai S, Okamoto S, Kawamura T, Hashimoto T. J Appl Crystallogr 1991;24:679.
[32] Toda A, Tomita C, Hikosaka M, Hibino Y, Miyaji H, Nonomura C, et al. Polymer 2002;43:947.